Composites Part B 79 (2015) 262–276

Contents lists available at ScienceDirect

Composites Part B

journal homepage: www.elsevier.com/locate/compositesb

Evaluation of sandwich panels with various polyurethane foam-cores and ribs

Hesham Tuwair [a], Matthew Hopkins [a], Jeffery Volz [b], Mohamed A. ElGawady [a, *], Mohaned Mohamed [c], K. Chandrashekhara [c], Victor Birman [d]

[a] Department of Civil, Architectural, and Environmental Engineering, Missouri University of Science and Technology, USA
[b] School of Civil Engineering and Environmental Science, The University of Oklahoma, USA
[c] Department of Mechanical and Aerospace Engineering, Missouri University of Science and Technology, USA
[d] Engineering Education Center, Missouri University of Science and Technology, USA

ARTICLE INFO

Article history:
Received 12 December 2014
Received in revised form
15 March 2015
Accepted 15 April 2015
Available online 23 April 2015

Keywords:
A. Foams
A. Glass fibres
C. Finite element analysis (FEA)
C. Analytical modeling

ABSTRACT

The objective of this study was to evaluate three potential core alternatives for glass fiber reinforced polymer (GFRP) foam-core sandwich panels. The proposed system could reduce the initial production costs and the manufacturing difficulties while improving the system performance. Three different polyurethane foam configurations were considered for the inner core, and the most suitable system was recommended for further prototyping. These configurations consisted of high-density polyurethane foam (Type 1), a bidirectional gridwork of thin, interconnecting, GFRP webs that is in-filled with low-density polyurethane foam (Type 2), and trapezoidal-shaped, low-density polyurethane foam utilizing GFRP web layers (Type 3). The facings of the three cores consisted of three plies of bidirectional E-glass woven fabric within a compatible polyurethane resin. Several types of small-scale experimental investigations were conducted. The results from this study indicated that the Types 1 and 2 cores were very weak and flexible making their implementation in bridge deck panels less practical. The Type 3 core possessed a higher strength and stiffness than the other two types. Therefore, this type is recommended for the proposed sandwich system to serve as a candidate for further development. Additionally, a finite element model (FEM) was developed using software package ABAQUS for the Type 3 system to further investigate its structural behavior. This model was successfully compared to experimental data indicating its suitability for parametric analysis of panels and their design.

1. Introduction

The majority of highway bridge decks are constructed with steel-reinforced concrete. The life-span of such materials can be significantly reduced by environmental conditions combined with wear from traffic, de-icing chemicals, and insufficient maintenance. As a result, transportation agencies have been endeavored to find new cost-effective, reliable construction materials. Fiber reinforced polymer (FRP) has shown great promise in eliminating corrosion concerns while also achieving a longer life-span with minimal maintenance [1]. FRP has been used for columns [2–4], beams [5,6], and panels [7–10]. FRP sandwich panels have many advantages, such as high flexural stiffness, strength, and environmental resistance, as well as reduced weight and life cycle cost. Using FRP deck panels should also contribute to accelerated bridge construction. These advantages make FRP sandwich panels an excellent candidate for construction of bridge decks.

Sandwich panels are often composed of two thin facings that are bonded to a much thicker core. The facings are typically made of high strength and stiffness material. The core usually consists of a rigid-foam, which has a low to moderate strength and stiffness [11]. However, the core design is industry-related. The facings are largely responsible for carrying flexural loads while the core provides shear capacity and integrity of the structure [12]. Many alternative forms of sandwich panels can be accomplished by combing different facings and core materials combined with varying geometries. As a result, optimum designs can be produced for specific applications [11].

* Corresponding author.
E-mail addresses: hrthw2@mst.edu (H. Tuwair), mshbq2@mst.edu (M. Hopkins), volz@ou.edu (J. Volz), elgawadym@mst.edu (M.A. ElGawady), mmm7vc@mst.edu (M. Mohamed), chandra@mst.edu (K. Chandrashekhara), vbirman@mst.edu (V. Birman).

http://dx.doi.org/10.1016/j.compositesb.2015.04.023
1359-8368/

Researchers and manufacturers have developed many FRP bridge deck designs with honeycomb and cellular cores made of E-glass reinforced polyester or vinyl ester resin. These designs have primarily been manufactured using filament winding, hand lay-up, and pultrusion methods [13]. A honeycomb core is one of the famous cores that being used in sandwich panels, implemented in bridge decks [8,14–20]. The honeycomb core consists of sinusoidal wave corrugations and straight components sandwiched between the facings. Testing showed that this type of panels is effective in providing high mechanical performance for minimum unit weight [14,19].

Researchers have proposed alternative forms for sandwich panels. Potluri et al. [21] proposed a conventional sandwich panel where the top and bottom facings were separated by a foam core. In their study, they introduced FRP stitches to improve the foam core performance. The stitches were used also to prevent core-to-facing debonding. It was found that both static and fatigue structural behavior can be improved by stitching together the top and bottom facings. Hassan et al. and Reis and Rizkalla [22,23] proposed an alternative system for FRP bridge decks. The proposed panel used three-dimensional fibers (stitches through foam cores) to connect the top and bottom GFRP facings. They observed that the delamination concerns were overcome. In addition, the fiber reinforced stitches increased significantly the core shear modulus. Dawood et al. [24] studied the fatigue behavior of sandwich panels with flexible and stiff cores. They found that the panels with flexible cores exhibit less degradation than those with stiffer cores due to the higher induced shear stresses at the same level of applied shear strain. Zureick [25] used finite element analysis to study different cross-sections of simply supported FRP decks. This study compared four different cross-sections, concluding that the box shaped and V shaped cores behaved much better than the other sections. Although the results from these studies provided a noteworthy understanding of FRP sandwich panel's behavior, most of these results cannot be extrapolated to other products.

The connection between the deck panels to the underlying steel girders is typically made using adhesive glue at the interface, shear studs, bolted connection, or steel clamps in a simply supported condition [26–29].

2. Paper scope and objectives

In the present study, small-scale FRP sandwich beams having three different foam core configurations (see Fig. 1) were investigated. The proposed system could reduce the initial production costs and the manufacturing difficulties while improving the system performance. The facings of the proposed three sandwich beams consist of E-glass woven fabric within a compatible polyurethane resin. Each configuration uses polyurethane foam as an infill material for the inner core. The investigated core configurations include high-density polyurethane foam (Type 1), a gridwork of thin, interconnecting, GFRP webs that is infilled with low-density polyurethane foam (Type 2), and GFRP trapezoidal-shaped infilled with low density polyurethane foam (Type 3). The polyurethane foam was chosen because it provides several advantages. These advantages include:

- Lower material and labor costs.
- Higher impact resistance and damping.
- Compatible material to the polyurethane resin, which aids in the infusion process and bonding with the face sheets.

A polyurethane resin system was used in the proposed sandwich beams as it has good high resistance and superior mechanical properties compared to polyester and vinyl ester [30]. This resin system was also chosen because it can reduce the initial costs of the sandwich beams. The one-step Vacuum Assisted Resin Transfer Molding (VARTM) process was also chosen to manufacture beams as it has a lower production cost than other manufacturing methods. For instance, the production cost of pultruded deck panels is approximately five times the production cost of hand lay-up deck panels [31]. The VARTM process can be used to manufacture both small and large FRP bridge deck panels. Although, polyurethane resin has a low pot life, recent modifications to the resin enabled it to be used with the VARTM process. A thermoset polyurethane resin with a longer pot life developed by Bayer MaterialScience was used in this study to manufacture the sandwich beams. All specimens were manufactured in the Composites Manufacturing Laboratory, Department of Mechanical and Aerospace Engineering, Missouri University of Science and Technology.

One of the greatest challenges faced by structural sandwich beams/panels is that the inner core has low transverse stiffness and strength. As a result, these panels are vulnerable to in-plane shear, wrinkling instability, and face-to-core deboning [32]. Therefore, the three design criteria considered in this study were chosen to improve the core's mechanical performance. The high-density foam in the first type was used with no webs in the core in an attempt to minimize both weight and cost. The cores in the second and third types consisted of low-density foam to minimize the weight reinforced with GFRP webs. Furthermore, the web elements of Types 2 and 3 potentially will delay both delamination failure and local crushing.

This paper compares the structural characteristics of the three proposed sandwich beam systems. The compressive and tensile strengths were assessed through the flatwise compressive and tensile tests of small sandwich cubes and coupon tests. The flexural strength and bending stiffness of each core system were also evaluated through three and four-point bending tests. The possible modes of failure of the different core configurations were also determined. A finite element model (FEM) was also developed for the Type 3 system and verified using the experimental results. The FEM was used for a better understanding of the structural behavior of this sandwich beam type.

A full-scale of Type 3 system was recently manufactured by the Structural Composites, Inc [33]. Based on the manufacturer, the resulting costs of the panel system was less than one half the cost of a comparable honeycomb FRP deck construction. Additionally, on a production run for an actual bridge, the manufacture estimates a further decrease in unit costs of 40%–50%, bringing the FRP deck alternative in line with initial costs of reinforced concrete decks.

3. Experimental program

This study examined the cross-sections of three different configurations of the closed-cell polyurethane infill-foam beams (see Fig. 1). The facings of the three types consisted of three plies of bidirectional E-Glass woven fabric (WR18/3010) infused with a compatible polyurethane resin. The core of Type 1 was comprised of high-density polyurethane foam that had a mass density of 96 kg/m^3. The Type 2 core consists of thin, interconnecting, glass fiber/resin webs that form a bidirectional FRP gridwork that is infilled with a low-density polyurethane foam of 32 kg/m^3. The Type 3 core was comprised of a trapezoidal-shaped, low-density, polyurethane foam and three-ply web layers (E-BXM1715).

The dry fabric and foam were stacked together in a rigid aluminum mold. High permeability layers placed over the fibers reduced infusion time, and a standard peel ply prevented the resin from adhering to the vacuum bag. Then, the thermoset polyurethane resin was infused through the vacuum-assisted process.

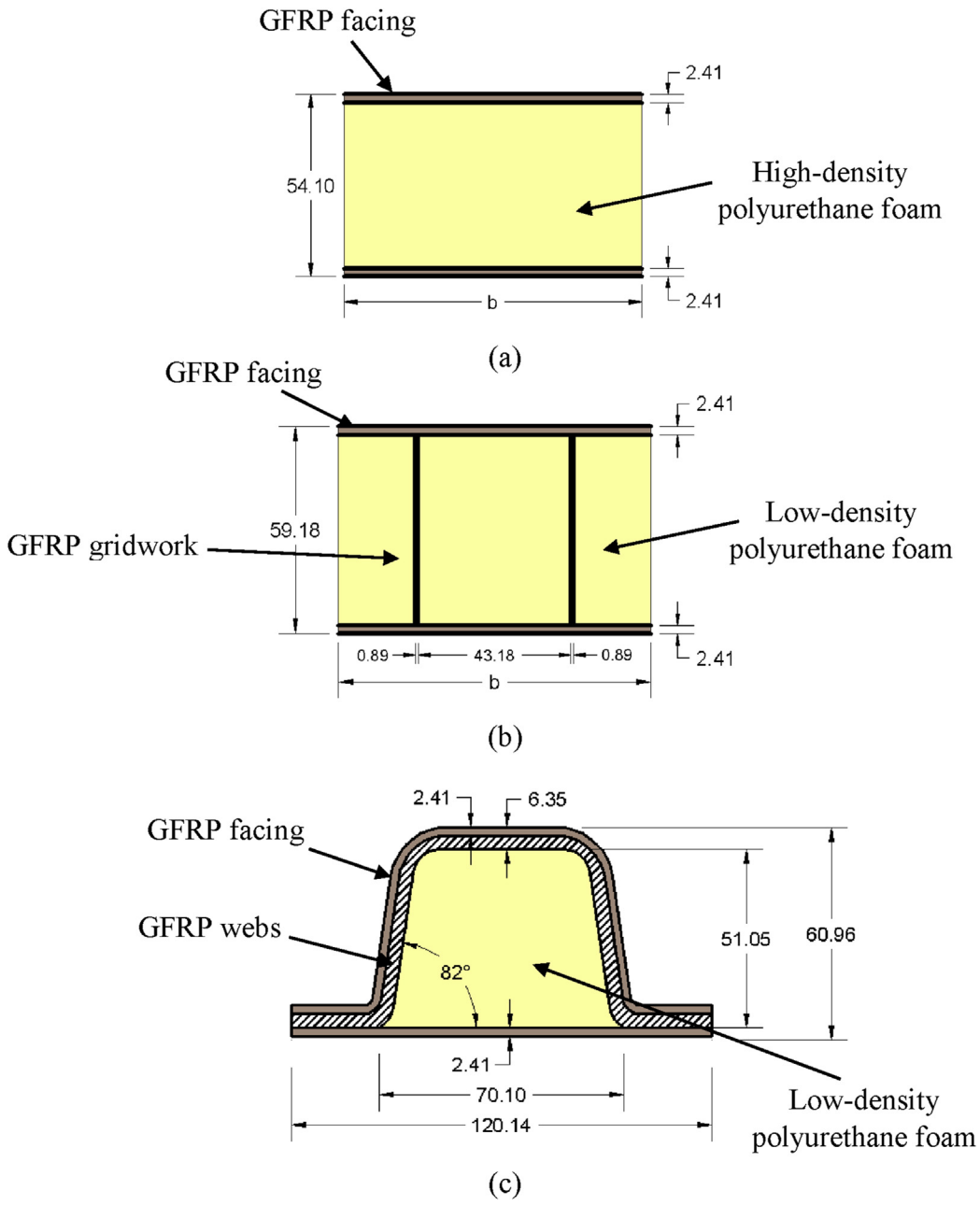

Fig. 1. Sandwich panel configurations for (a) Type 1, (b) Type 2, and (3) Type 3. (all dimensions are in mm).

The resin was cured for 1 h at 70 °C and for 4 h at 80 °C in a walk-in oven.

In the following sections detailed descriptions of the tests carried out on material characterization and small-scale sandwich structures are reported. The material characterization included flatwise tensile and compressive tests on the GFRP facings and web layers, and flatwise compressive tests on the two types of polyurethane foam. The tests on small-scale sandwich structures involved flatwise compressive and tensile tests and three and four-point bending tests.

3.1. Material characterization

3.1.1. Polyurethane foam core

Polyurethane closed-cell foam was used for the three types of cores. The ASTM C365 standard [34] was applied to conduct flatwise compression tests of the foams (Fig. 2a). Three cubes of high-density polyurethane foam and three cubes of low-density polyurethane foam were tested to determine the compressive properties. The coupon dimensions and mechanical properties of the tested specimens are listed in Table 1. Because the foam is quite sensitive to displacement, the tests were conducted in an Instron 4469 testing machine, which can measure the response at small displacements. All specimens were tested under displacement control at a loading rate of 2.54 mm/min.

3.1.2. GFRP facings and web layers

The ASTM D3039 standard [35] was employed to determine the tensile properties of the GFRP laminates extracted from the beams' facings and web cores. All specimens were 254 mm long and 25.40 mm wide. The coupon thicknesses were 2.41 mm and 3.94 mm for the facing and web layers, respectively. End tabs

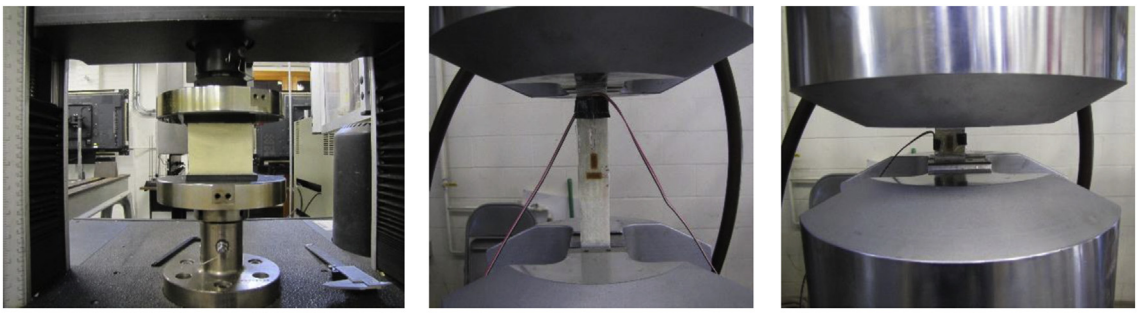

Fig. 2. Test setup for (a) flatwise foam compressive test, (b) tensile coupon test, and (c) compressive coupon test.

Table 1
Polyurethane foam properties from compressive tests.

Foam density	Width (mm)	Length (mm)	Thick. (mm)	Elastic modulus (MPa)			Compressive strength (MPa)			Compressive strain (mm/mm)		
				Mean	S.D*	C.V*	Mean	S.D	C.V	Mean	S.D	C.V
Low	64.26	65.79	69.34	2.1	0.15	7.1	0.056	0.0034	6.9	0.025	0.005	21.4
High	88.90	88.90	49.28	37.1	4.63	12.5	1.04	0.0100	1.0	0.037	0.003	7.7

*S.D: Standard deviation.
*C.V: Coefficient of variation (%).

holding the specimen were 63.50 mm long. The tension test was conducted in an MTS-880 testing machine (see Fig. 2b) with a loading rate of 1.27 mm/min. The longitudinal strains were recorded using electrical strain gauges of 350 Ω at the middle of the coupons. Three coupons from the facings and three from the web core were also tested in compression (see Fig. 2c), according to the ASTM D3410 standard [36]. The coupon dimensions used in compressive tests were 147.32 mm long and 25.40 mm wide; the gauge length was 20.32 mm. The displacement rate of the test was set to 0.127 mm/min. Two strain gauges were attached to the gauge length between the end taps was 147.32 mm long and 25.40 mm.

3.2. Small-scale sandwich structures characterization

3.2.1. Flatwise compressive tests

Six specimens were tested: three for Type 1 and three for Type 2. Flatwise compressive strength and elastic modulus for the sandwich core's structural design properties were determined using MTS-880 universal testing machine and following ASTM C365 standard [35] (see Fig. 3a). Since the main purpose of the low-density polyurethane foam of the Type 3 core is its use as a mold for the trapezoidal-shaped FRP layers, the bare foam was tested without any FRP, as demonstrated in the material characterization section. Specimens of Types 1 and 2 had a constant square cross-section of 88.90 mm × 88.90 mm corresponding to a cross-sectional area of 7903 mm^2 which was smaller than the 10,323 mm^2 area recommended by the ASTM C365 [34]. The composite thickness of Type 1 and 2 was 54.10 mm and 59.18 mm, respectively. Each specimen was centered under the loading plate to ensure a uniform load distribution. The speed of the crosshead displacement was set at a rate of 2.54 mm/mm.

3.2.2. Flatwise tensile tests

MTS-880 universal testing machine was used to conduct the flatwise tensile tests (Fig. 3b) according to the ASTM C297 standard [37]. Six specimens were tested (three for Type 1 and three for Type 2) to determine the flatwise tensile strength of core. This test also provided information on the quality of the core-to-facing bond. Similar to the flatwise compression tests, Types 1 and 2 had a constant square cross-section of 88.90 mm × 88.90 mm corresponding to a cross-sectional area of 7903 mm^2, which was larger than 645.16 mm^2 recommended by the ASTM C297 [37]. The composite thickness of Type 1 and 2 was 54.10 mm and 59.18 mm, respectively. In order to be gripped in the test frame, each specimen was adhesively bonded to T-shape steel sections with an epoxy adhesive supplied by the 3M Company. The loading rate was set at 1.27 mm/min.

3.2.3. Flexural tests

Three-point bending tests were conducted on short beams and four point bending tests on long beams in accordance with ASTM C393 standard [38]. The test setup is illustrated in Fig. 4. A Wyoming test fixture (model no. CU-LF) was used [39]. Thick steel plates and high resistance rubber pads (with a shore A hardness of 60) were inserted at the loading and supporting points to distribute the load uniformly and reduce the stress concentrations. The load was applied using an Instron 4469 testing machine with a load capacity of 50 kN and a displacement rate of 1.27–2.54 mm/min. All specimens were tested under displacement control.

The objective of the three-point bending test is to generate the shear stresses by using relatively short beams and analyze their impact on the total deflection. A total of nine short beams were investigated: four for Type 1, four for Type 2, and one for Type 3. Each specimen was tested over a clear span of 152.40 mm with the load applied at the center of the beam (see Fig. 4a). Four-point bending tests were conducted (Fig. 4b) to investigate the effect of the three types of cores on flexural behavior of the sandwich beams by increasing the span length. Three specimens of each type were investigated, i.e. a total of nine sandwich beams were examined. They were tested in one-way bending with the span of 609.60 mm, under two equal point loads, applied at 203.20 mm from each support. The specimens were loaded to failure at a displacement rate of 1.27–2.54 mm/min.

Strains in the axial direction of the beams were measured with electrical, high precision strain gauges (produced by Micro Measurements Group) at a resistance of 350 Ω. The bottom deflection at

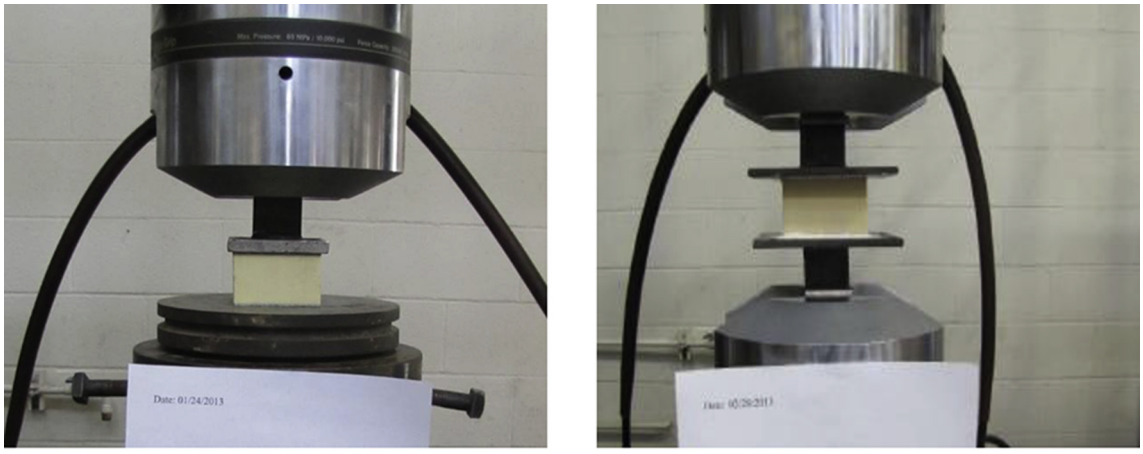

Fig. 3. Test setup for flatwise sandwich: (a) compressive test, and (b) tensile test for Type 1.

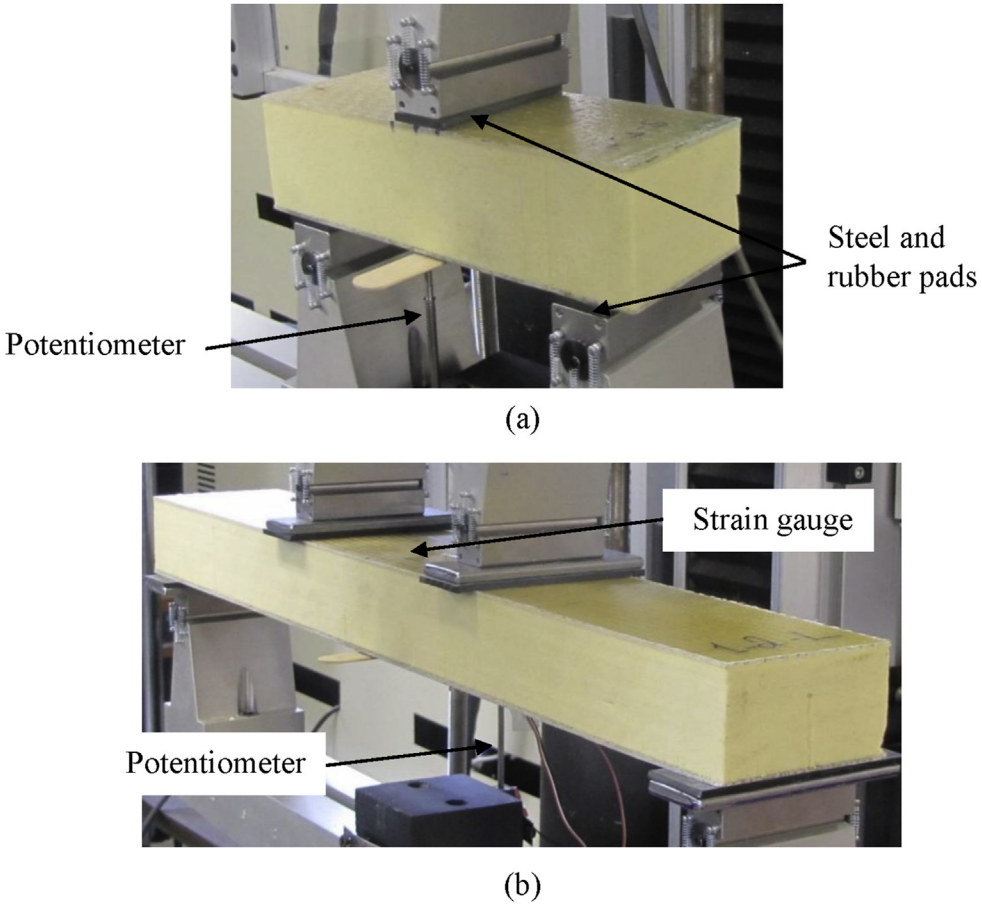

Fig. 4. Test setup for (a) three-point, and (b) four-point bending tests for Type 1.

mid-span was recorded using a Linear Potentiometer (LP). A Linear Variable Differential Transducer (LVDT) was mounted on the movable frame of the machine to monitor top deflection at mid-span. The long beams, used for the four-point bending, had gauges attached to the top and bottom of the facesheet surface at the middle of the beam. The short beams, used for the three-point bending, had one gauge attached at the bottom of the facesheet surface (at the middle of the beam). A data acquisition system was used to record the load, displacement, and strain during testing.

4. Assessment of flexural stiffness (EI)

The flexural stiffness (EI) where E is the equivalent modulus of elasticity and I is the equivalent moment of inertia of the sandwich

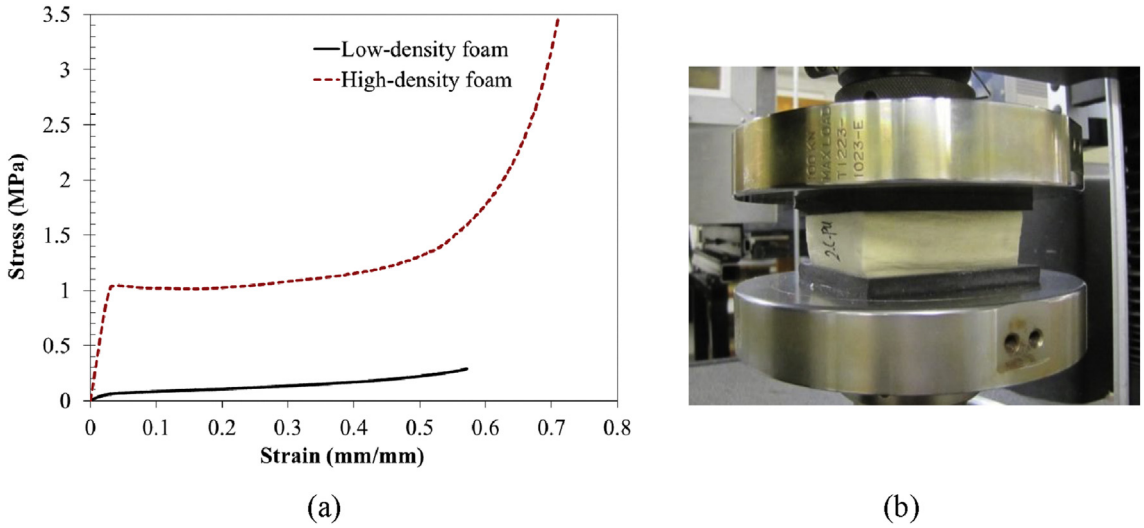

Fig. 5. Flatwise foam compressive test: (a) stress–strain curves, and (b) specimen during testing.

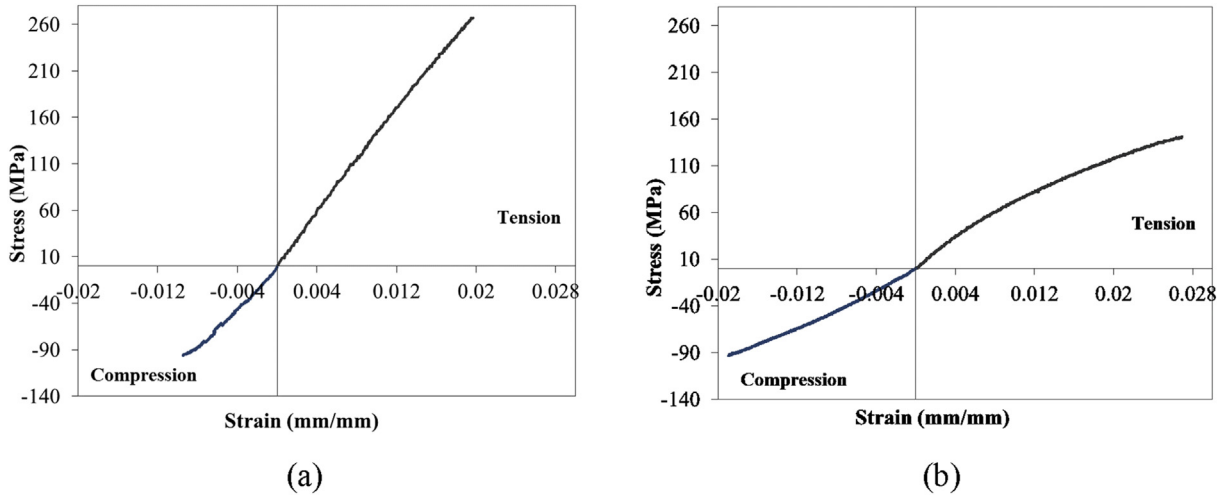

Fig. 6. Stress–strain curve for (a) GFRP facing, and (b) web layers.

beam was examined because it is typically the driving factor when designing sandwich panels. The flexural stiffness of each beam was calculated using First-order Shear Deformation Theory (FSDT) [40]. These results were used to compare the flexural stiffness of beams with different core types. The FSDT was also used to estimate the shear stiffness of each sandwich beam type by fitting the results collected from three and four-point flexural tests. Note that it is also possible to estimate the flexural by utilizing the well-known Newmark's equation [41] and the analytical solutions proposed by Faella et al. [42].

In the FSDT analysis, the polyurethane foam and GFRP bidirectional woven fabric facings were modeled as isotropic materials. A perfect bond was assumed to exist between the core and the facings as well as between the core and webs. The bending stiffness was computed accounting for the deflection components that are associated with bending and shear deformations. Given the mid-span deflection values from the three-point loading and four-point loading tests as well as the applied point load (P) and using the following FSDT equations, the shear stiffness GA and flexural stiffness (EI) were determined from Ref. [40]:

$$\Delta_{midspan} = \frac{PL^3}{48EI} + \frac{PL}{4kGA} \quad \text{for three} - \text{point loading test} \qquad (1)$$

Table 2
GFRP properties from tensile coupon tests.

Coupon type	Width (mm)	Thick. (mm)	Tensile Modulus (MPa)			Ultimate strength (MPa)			Ultimate strain (mm/mm)		
			Mean	S.D	C.V	Mean	S.D	C.V	Mean	S.D	C.V
Facing	25.40	2.89	13,977	131.7	0.94	264.8	15.9	6.1	0.019	0.001	5.88
Web core	25.40	3.94	11,803	938.4	7.95	137.9	6.2	4.51	0.027	0.004	13.82

Table 3
GFRP properties from compressive coupon tests.

Coupon type	Width (mm)	Thick. (mm)	Compressive modulus (MPa)			Ultimate strength (MPa)			Ultimate strain (mm/mm)		
			Mean	S.D	C.V	Mean	S.D	C.V	Mean	S.D	C.V
Facing	25.40	2.89	13,233	1711	12.9	102.7	16.27	15.80	0.011	0.004	34.66
Web core	25.40	3.94	5732	860	15.0	101.4	8.41	8.27	0.023	0.004	17.26

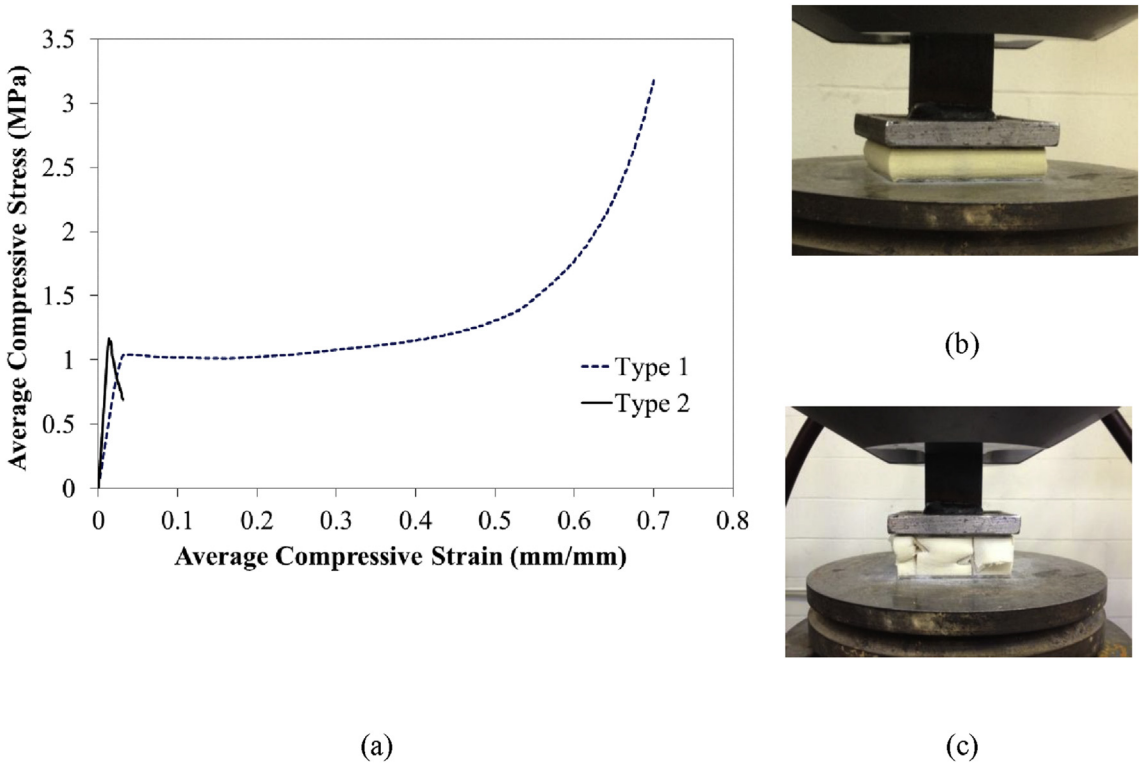

Fig. 7. Flatwise sandwich compressive tests: (a) stress–strain curves, (b) failure mode of Types 1, and (c) failure mode of Types 2.

$$\Delta_{midspan} = \frac{23PL^3}{1296EI} + \frac{PL}{6kGA} \quad \text{for four} - \text{point loading test} \qquad (2)$$

where L is the span length and k is the shear correction factor (which was assumed to be 5/6).

5. Experimental results

5.1. Material characterizations

5.1.1. Polyurethane foam core

Fig. 5a illustrates the average compressive stress–strain curves of the tested low (soft) and high-density (rigid) polyurethane foam cubes. These curves are linear in the elastic region, with a yield region at an average stress of 0.056 MPa for the low-density foam and 1.04 MPa for the high-density foam. The yield behavior can be explained by the buckling of the foam's internal walls. A long flat plateau was followed. Then, a densification (hardening) region was created by a gradual stress increase when the cell walls were stacked prior to final densification. No visible signs of failure were observed (see Fig. 5b). Residual displacement of the collapsed foam did, however, occur once the unloading stage was complete.

5.1.2. GFRP facings and web layers

Fig. 6a illustrates average axial tensile and compressive stress–strain curves for the GFRP facing. In the tensile test, the facing exhibited a linear elastic response up to strain of 0.019 mm/mm at an ultimate stress of 264.7 MPa. In the compressive test, the ultimate compressive strength was 102.73 MPa, or 38.8% of its

Table 4
Summary of flatwise sandwich compressive tests.

Panel type	Results	Width = length (mm)	Thick. (mm)	Yield strength (MPa)	Yield strain (mm/mm)	Compressive modulus (MPa)
Type 1	Average	88.90	54.10	1.04	0.034	37.1
	S.D			0.011	0.003	4.6
	C.V			1.01	7.76	12.5
Type 2	Average	88.90	59.18	1.18	0.016	75.3
	S.D			0.030	0.004	12.8
	C.V			2.55	24.54	16.9

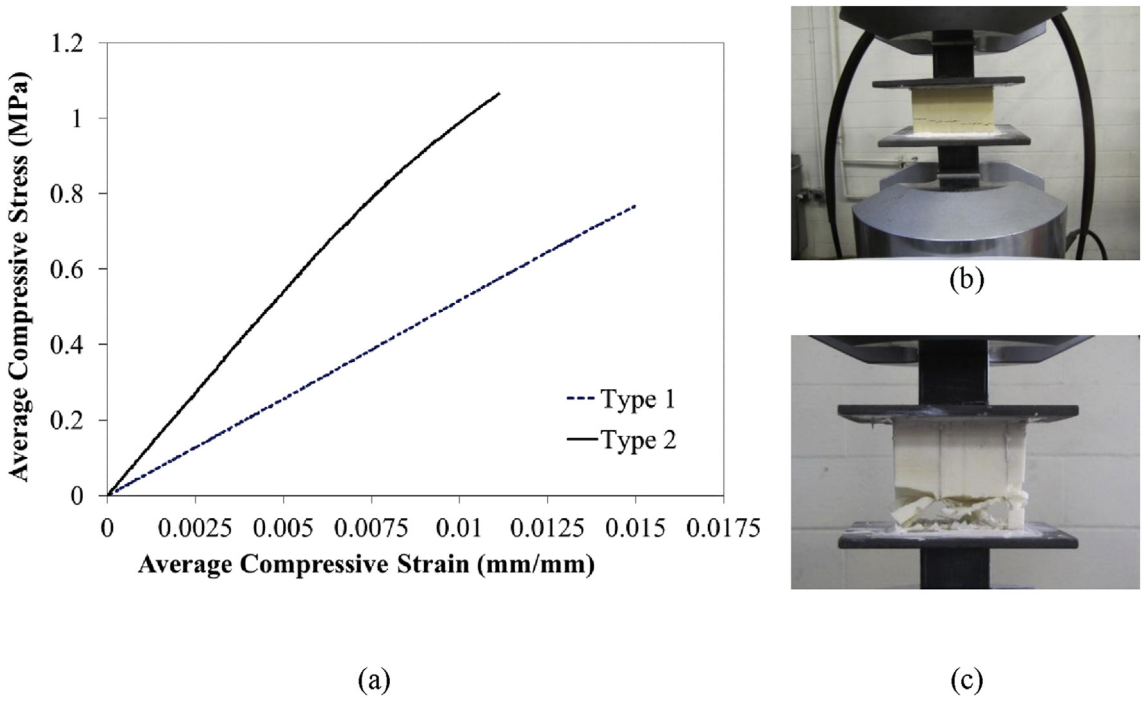

Fig. 8. Flatwise sandwich tensile tests: (a) stress–strain curves, (b) failure mode of Types 1, and (c) failure mode of Types 2.

Table 5
Summary of flatwise sandwich tensile tests.

Panel type	Results	Width = length (mm)	Thick. (mm)	Ultimate strength (MPa)	Ultimate strain (mm/mm)	Tensile Modulus (MPa)
Type 1	Average	88.90	54.10	0.79	0.016	47.23
	S.D			0.024	0.001	0.49
	C.V			3.09	5.91	1.03
Type 2	Average	88.90	59.18	1.12	0.012	96.80
	S.D			0.35	0.001	19.87
	C.V			31.14	10.20	20.53

Table 6
Test results of three-point bending tests.

Panel type	Results	Width [b] (mm)	Depth (mm)	Span (mm)	P_u (kN)	Δ_u (mm)	ε_{max} (mm/mm)	Failure mode
Type 1	Average	76.45	54.10	152.40	5.16	8.64	0.0060	Indentation + crushing
	S.D				0.34	0.66	0.0008	
	C.V				6.62	7.68	14.48	
Type 2	Average	76.45	59.18		6.27	1.12	0.0023	Buckling
	S.D				1.28	0.25	0.001	
	C.V				20.47	23.39	43.56	
Type 3	–	See Fig. 1	60.96		21.12	6.10	0.0054	Wrinkling

ultimate tensile strength. Fig. 6b presents average axial tensile and compressive stress–strain curves of the web layers of the Type 3 beam. The curve exhibited nonlinear behavior due to re-orientation of +45/-45 fibers. The ultimate tensile strain was 0.027 mm/mm corresponding to the ultimate stress of 137.9 MPa. In the compression region, the ultimate compressive strength was 102.73 MPa, or 73.5% of its ultimate tensile strength. These properties were also valid in the transverse direction for both the facings and the web layers due to the symmetric quasi-isotropic architecture of the reinforcing fibers. The observed failure mode for the facing and web layer coupons under tension was a sudden kink rupture and shear rupture, respectively. All tested coupons failed due to micro buckling and kinking of the fibers under compression. A summary of the results collected from the coupon tests is contained in Tables 2 and 3.

5.2. Small-scale sandwich structures characterization

5.2.1. Flatwise compressive tests

Flatwise compressive tests were conducted on sandwich cubes for the first two types to examine the properties of their cores. Fig. 7a displays the compressive stress–strain responses for Types 1 and 2. For Type 1, the curve follows a typical behavior of cellular materials [43]. The first part of the curve was linear in the elastic region, followed by the plateau region where the stress was almost constant under increasing deformation. Then, there was a sharply increasing loading region at a large strain corresponding to solidification. The yield region occurred at an average stress of 1.04 MPa. This yield behavior was attributed to buckling of the foam's internal cell walls. The flat plateau was produced by the development of localized buckling within the cell walls. As the deformation

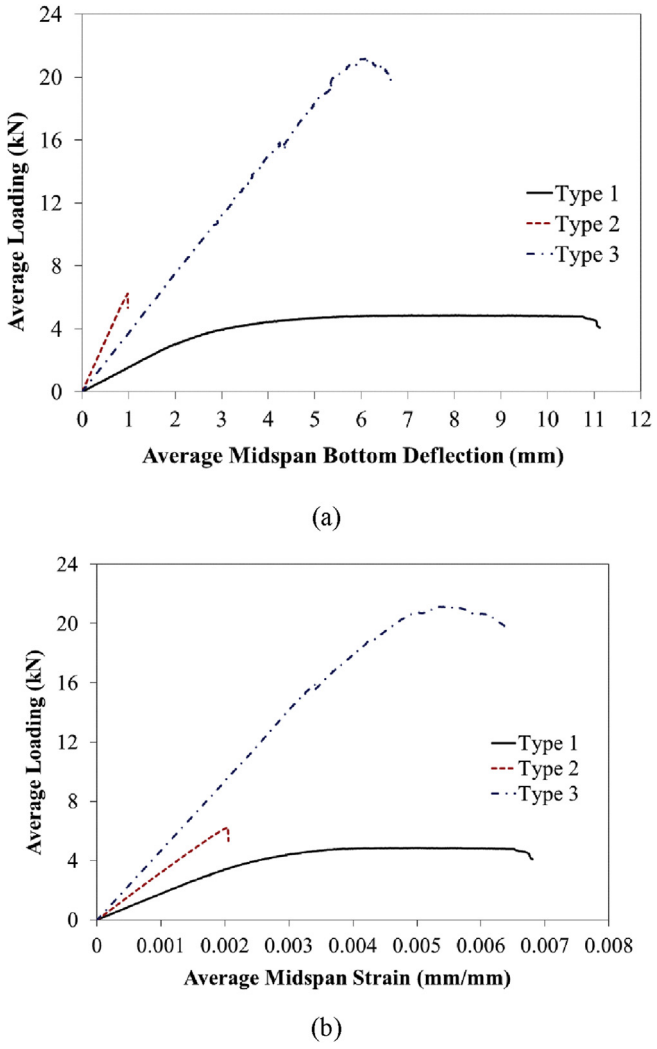

Fig. 9. Three-point bending tests: (a) load vs. mid-span deflection, and (b) load vs. mid-span bottom strains.

increased, the cell walls stacked on top of each other resulting in the closure of most of the voids. Therefore, the foam became densified and displayed higher strength. A deformed shape of the Type 1 foam is shown in Fig. 7b. For Type 2, the stress–strain curve illustrates that the web core foam initially exhibited a nearly linear behavior up to the maximum stress, which had an average value of 1.18 MPa. It was noticed that the failure mode of this type was buckling of the thin FRP webs and subsequent delamination between the foam and the webs, as shown in Fig. 7c. A summary of the test results for Types 1 and 2 is presented in Table 4.

5.2.2. Flatwise tensile tests

The flatwise tensile properties of the first two types of the sandwich cubes were determined. Fig. 8a presents the stress–-strain curves for Types 1 and 2. For Type 1, the response was linearly-elastic up to failure. The failure mode for all of the tested Type 1 specimens was cohesive rupture of the core, which displayed a cup-cone surface (Fig. 8b). The average ultimate tensile strength and the ultimate tensile strain were approximately 0.79 MPa and 0.016 mm/mm, respectively. These results are summarized in Table 5. For Type 2, the curve was linearly elastic up to a strain of 0.0076 mm/mm. Beyond this strain, the response became slightly nonlinear until the specimen ruptured. This nonlinearity was produced by the foam's contribution to tensile resistance. The average ultimate stress and strain were 1.12 MPa and 0.012 mm/mm, respectively. Because of low strength and stiffness of the low-density foam, the initial failure of the foam was Mode I fracture characterized by horizontal cracks. Then, a debonding between the FRP gridwork and the facing occurred, as observed in Fig. 8c.

5.2.3. Flexural behavior

Table 6 summarizes the results gathered from the three-point bending tests. Fig. 9a presents the load deflection curves at the mid-span for the three core types. For Type 1, all sandwich beams exhibited a linear behavior up to a deflection of approximately 2.79 mm. At larger deflections nonlinearity occurred with stiffness softening up to failure. This behavior can be attributed to the crushable nature of the polyurethane foam. The average of the maximum vertical deflection and the longitudinal bottom strain that were recorded at mid-span were 8.64 mm and 0.006 mm/mm, respectively, at a failure load of 5.16 kN. The recorded strains (see Fig. 9b) at the bottom mid-span exhibited behavior similar to that of the deflection response. As can be observed from the strain curve, the maximum strain value was significantly lower than the ultimate strain of the GFRP facing, which is attributed to the observed failure mode. All specimens failed due to an inward local bending of the compression facing beneath the loading point, as shown in Fig. 10a, followed by crushing in the top facing and the foam (Fig. 10b). The local bending occurred because the foam's compressive strength and stiffness are insufficient to resist high local stresses.

Type 2 specimens were loaded up to failure. It should be noted from Table 6 that the standard deviation of this type is relatively high. This can be attributed to the distribution of transverse webs as each specimen had a different arrangement due to cutting it from a different location from the large panel. The curve in Fig. 9 suggests a nearly linear response up to failure. The average of the maximum deflection and longitudinal strain recorded at mid-span were 1.12 mm and 0.0023 mm/mm, respectively, at an average failure load of 6.27 kN. The initial failure mode was buckling of the FRP webs coupled with compressive failure in the foam, as depicted in Fig. 10c. Due to post buckling deformations of the webs, the webs subsequently fractured, and the top facing wrinkled inward.

For Type 3 specimens, due to a limited amount of trapezoidal polyurethane foam available, only one specimen was tested. Fig. 9a illustrates the tested beam's load-deflection response. In a manner similar to the other two types, the Type 3 specimen also exhibited a linear behavior up to failure as reflected in the strain gauge reading in Fig. 9b. The average of the maximum deflection recorded at mid-span was approximately 6.10 mm at failure load of 21.12 kN. The sandwich beam initially failed by delamination between the web layers and the foam at one corner. The ultimate failure mode included wrinkling of the top facing. This wrinkling was followed by crushing of the web layers under the loading point (see Fig. 10d). It should be noted that the stiffness of the Type 3 curve was slightly lower than of the Type 2, a result that was not anticipated. Overall, these tests revealed that local failures, rather than global shear failures dominated flexural response. The results provided load versus displacement responses which were needed to estimate the flexural stiffness of each sandwich type.

Table 7 summarizes the results collected from the four-point bending tests. These results were presented in terms of the ultimate load, deflection, and strain in both the upper and lower facings at the ultimate load, and the observed failure modes. Fig. 11a presents a load-deflection curve for each of the three types tested. The behavior of each type clearly demonstrated the significant effect produced by the type of core used. In general, all beam types

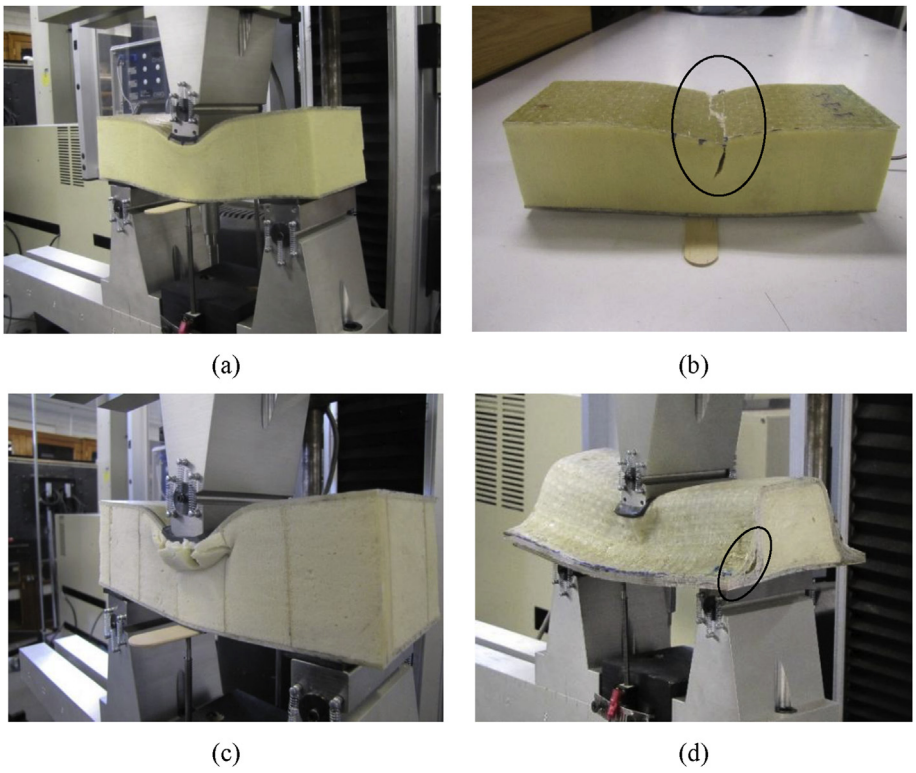

Fig. 10. Failure modes: (a) local buckling, (b) crushing of the top facing and foam in Type 1, (c) buckling of the webs and compressive failure in the foam in Type 2, and (d) wrinkling of the top facing and crushing of the webs in Type 3.

Table 7
Test results of four-point loading tests.

Panel type	Results	Pu (kN)	Width [b] (mm)	Depth (mm)	Span (mm)	Δ_u (mm)	Bottom-face ε_{max} (mm/mm)	Top-face ε_{max} (mm/mm)	Failure mode
Type 1	Average	7.0	102.11	54.10	609.60	21.08	0.0037	−0.0038	Bending fracture or shear failure
	S.D	0.14				1.21	0.0003	0.0006	
	C.V	1.94				5.71	6.63	15.87	
Type 2	Average	12.2	105.66	59.18		13.21	0.0061	−0.0092	Intercellular buckling + shear failure
	S.D	3.0				2.42	0.0018	0.0028	
	C.V (%)	24.76				18.36	30.83	30.75	
Type 3	–	19.1	See Fig. 1	60.96		14.22	0.0046	−0.0045	Compression failure

behaved linearly until a certain load. The linear behavior was followed with a nonlinear response that was produced by shear deformation of the polyurethane core. Nonlinearity in the strain curves (see Fig. 11b) was not observed because strain measurements were taken at the facing surface, reflecting the facing's linear behavior. The maximum strains measured on both the compression and tension facings were significantly lower than the ultimate strain measured in the compression and the tension coupon specimens (0.019), which is also attributed to each beam because the strength of the facing materials is high, so that it would be impossible to cause compressive or tensile failure at this span length.

The average mid-span recorded deflection for the Type 1 specimens was 21.10 mm at an approximate ultimate load of 7.0 kN. The initial failure mode occurred when the core yielded under the loading points and the top face sheet wrinkled. All Type 1 sandwich beams exhibited either a bending fracture in the top facing or a shear failure in the core followed by debonding (see Fig. 12a and b, respectively). The top facing in Type 2 initially failed due to intercellular buckling (Fig. 12c). Shear failure in the core material (Fig. 12d) was the ultimate failure mode. As shown in Table 7, the ultimate loads had a high degree of variability. This variability was attributed to the number of longitudinal webs within each specimen; one specimen had three longitudinal webs, and the other two had two. The maximum measured deflection at mid-span for the Type 3 specimens was 14.22 mm at an ultimate load of approximately 19.10 kN (Fig. 11a). The behavior was linear with a subsequent softening nonlinear response prior to reaching the ultimate load capacity. This softening nonlinearity could be attributed to compression failure under the loading points and associated nonlinear response of the foam (Fig. 12e). The ultimate failure was caused by excessive compressive stresses in the webs, which created a hinge mechanism in the top facing under the loading point (Fig. 12f).

5.3. Stiffness (EI) calculations

Flexural stiffness of Types 1 and 2 was estimated using FSDT equations (1) and (2), and the results are listed in Table 8. The flexural stiffness for Type 3 was based on the deflection associated with bending from the four-point loading test only. The shear stiffness, based on the geometry of Type 3, was expected to be very

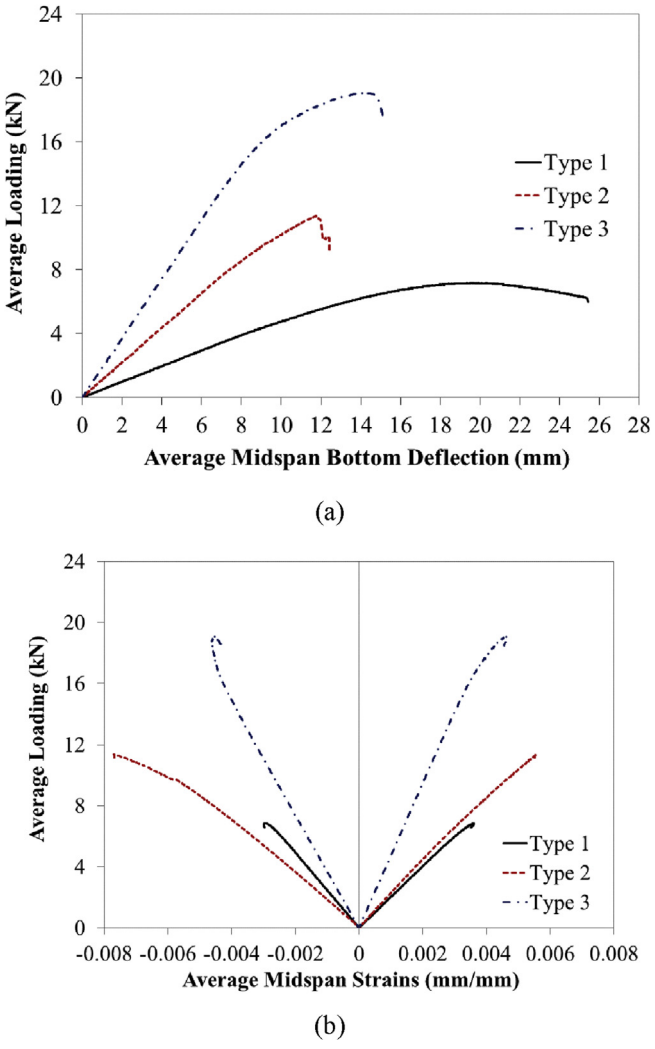

Fig. 11. Four-point bending tests: (a) load vs. mid-span deflection, and (b) load vs. mid-span top and bottom strains.

large. Therefore, shear deformations can be assumed a relatively small percentage of the total deflection as proved by Tuwair et al. [44]. As a result, the Euler-Bernoulli beam theory was used for this type and provided reasonable accuracy.

Since each type had a different geometry, the results were normalized to their widths and weights for comparison purposes (Table 9). When the results were compared to each other, the Type 3 specimens supported higher load at failure. In terms of stiffness per unit width, Type 3 beams outperformed Type 1 and Type 2 beams by 2.38 and 1.79 times, respectively. In terms of weight comparisons, the corresponding flexural stiffness ratios were 2.32 for Type 2 beams and 2.38 for Type 1 beams. A comparison was also made between Type 3 sandwich beam and conventional reinforced concreted (RC) beam of similar cross-sectional dimensions. Notably, Type 3 weigh approximately one-fifth of the RC beam that made of normal weigh concrete. In addition, the RC beam with 27.6 MPa compressive strength would be 4.4 stiffer than Type 3 sandwich beam.

The relative contributions of shear to the total deflection was 63%, 34%, and ~1% for Types 1, 2, and 3, respectively. Therefore, in Type 1 without ribs in the core, shear deformation of the polyurethane foam contributed over half of the total deflection. Evidently this highlights the importance of shear deformation to the total deflection in Type 1. In contrary, the web layers in Type 3 core contributed significantly to the shear stiffness of the of the sandwich beam practically eliminating shear deformations.

As a result, the Type 3 beams are recommended in this study because they:

- Possess the highest flexural strength, flexural stiffness, and shear stiffness.
- Demonstrate excellent bond between the core and facings.
- Did not suffer significantly from localized effects at concentrated loads.
- Produce a more gradual failure compared to the other types, which failed instantaneously.

6. Discussions

The flatwise compressive tests revealed that the Type 2 core was significantly stronger and stiffer than the Type 1 core. These results also revealed excessive deformations under concentrated loads, potentially leading to serviceability issues. The flatwise tensile tests were used to examine the bond quality between the core and the facings. In Type 1, failure occurred in the polyurethane foam itself, as the bond between the foam and the facing was stronger than the foam core. On the other hand, the Type 2 core failed at the bond between the core and the facings. This occurred due to the higher tensile capacity of the used interconnected GFRP gridwork compared to Type 1 where the tensile stresses were resisted by the foam core only.

The results gathered from the three-point bending tests revealed that in all three types tested, the localized failure under concentrated loads was the critical concern. These local failures led to the stiffness reduction identified in all force–displacement curves prior to final failure. The compressive failure of Type 1 was attributed to the foam's low stiffness and strength. The localized buckling of the thin core webs that occurred in Type 2 was the result of the high aspect ratio of these elements. The initial failure by delamination occurred in Type 3 because of the specimen manufacturing defects. Type 3 specimen finally failed when the top facing wrinkled under the loading point. In four-point loading tests all specimens behaved linearly until yielding, intercellular buckling, and compression failure occurred. Nevertheless, the Type 1 specimens were influenced by localized effects more than the Types 2 and 3. Types 2 and 3 failed in shear in the core and compression in the top facing, respectively, while Types 1 and 2 failed instantaneously with a loud sound, while Type 3 failed more gradually. The difference between the top and bottom deflections recorded at mid-span was much smaller for Type 3 than it was for the other two types. This reflects the local stiffness and strength of the web-reinforced sandwich panels. The web layers in Type 3 enhanced the section by providing support to the top facing and, thus, improved local stiffness and strength.

Serviceability limit state is a key criterion in designing sandwich bridge decks because of the relatively low stiffness of polyurethane composites (E-glass fibers and polyurethane resins). As stated in the stiffness (EI) calculations section of this study, the Type 3 beam possessed the highest flexural and shear stiffness. The web layers that were introduced to this type contributed significantly to the increase in the shear stiffness so that minimal shear deformation occurred. When normalized to the beam widths, the Type 3's core contributed substantially to its flexural stiffness increasing it by 238% and 179% in comparison to Types 1 and 2, respectively.

Overall, the Type 3 core is likely the most practical for implementation in bridge decking. Although meeting the serviceability requirements of bridge decking will require a larger cross-section, it will be achievable with reasonable facing and web layers

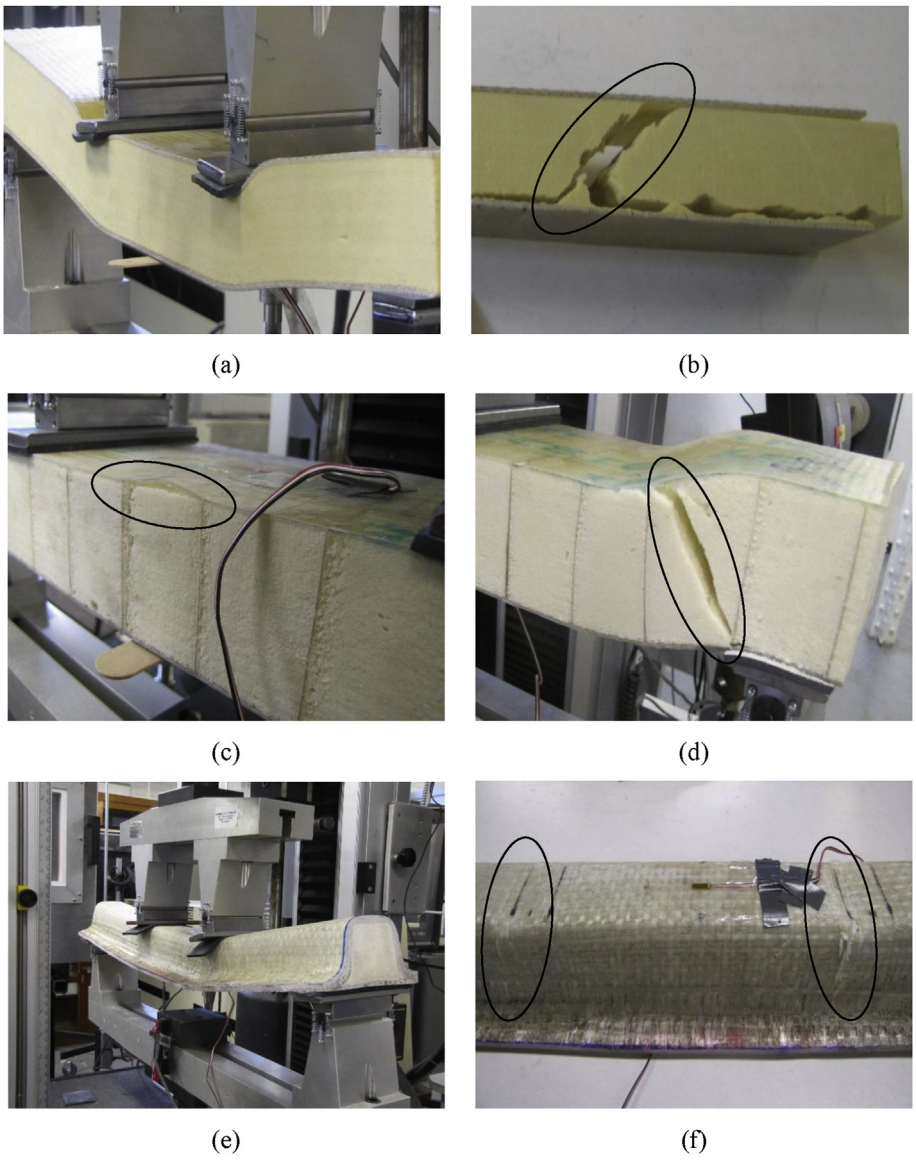

Fig. 12. Failure modes: (a) bending fracture, (b) shear failure in Type 1, (c) intercellular buckling, (d) shear failure in Type 2, (e) deformed shape during testing, and (f) compression failure under loading points in Type 3.

Table 8
Calculated stiffness results.

Panel type	Flexural stiffness (EI) (kN·mm^2)			Shear stiffness (GA) (kN)		
	Mean	S.D	C.V	Mean	S.D	C.V
1	5,056,821	650,934	12.9	91.7	1.3	1.4
2	6,549,876	1,014,418	15.5	391.2	25.1	6.4
3	8,865,849	–	–	~∞	–	–

thicknesses, as well as a smaller and more practical panel depth than in the other two construction types. The typical size of a full-scale deck panel is five feet wide by eight feet long. The span (2.44 m) of the panel will be perpendicular to the traffic direction and will be simply supported on the short dimensions (1.52 m). Thus, the system would behave as a flexural system in the perpendicular direction to traffic and as a truss system in the parallel direction. The design of the panel will be based on the standard AASHTO Truck or Tandem [45], whichever controls a particular aspect. In accordance with FHWA guidelines, panel stresses must be limited to 20% of the ultimate strength. Deflection should be limited

Table 9
Normalized stiffness values.

Panel type	Width (mm)	Mass density (kN/m^3)	EI/width (kN·mm^2/mm)	EI/mass-density (kN·mm^2/(kN/mm^3))
1	102.11	203.2	44,9412	24,886
2	105.66	208.4	59,691	31,429
3	83.06	484.4	106,740	18,302

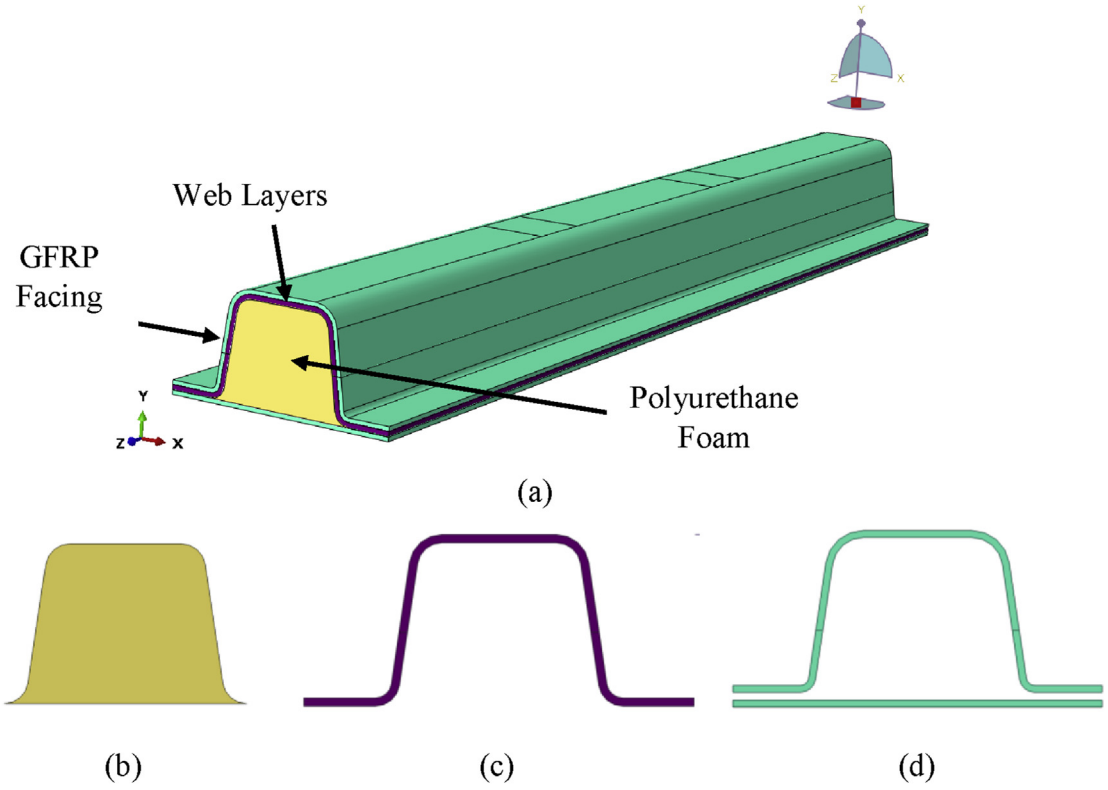

Fig. 13. FE model: (a) overall FE model perspective of the tested panel, (b) polyurethane foam, (c) web layers, and (d) GFRP facings.

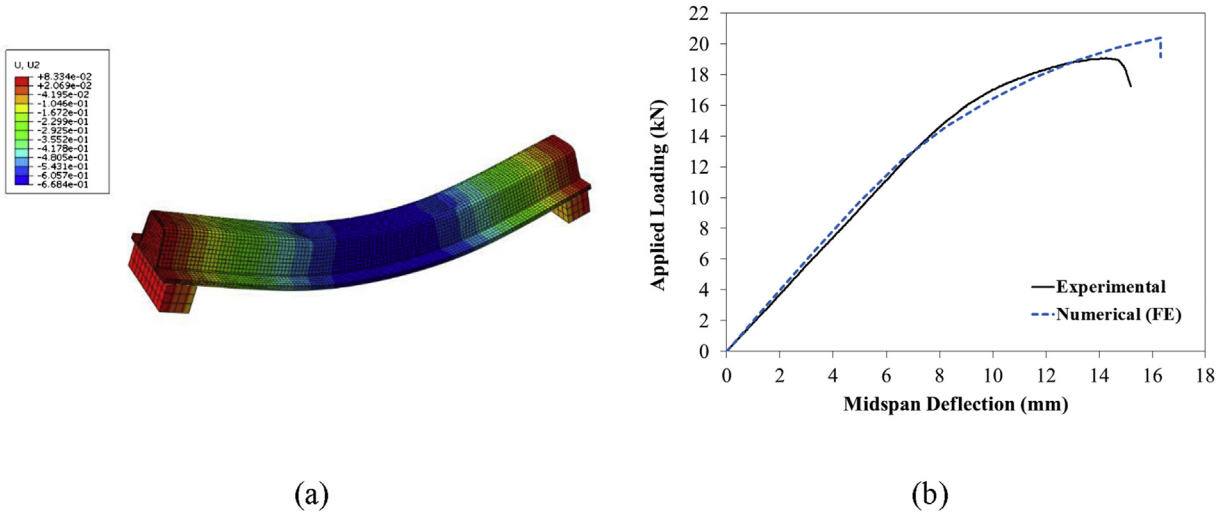

Fig. 14. Results of FEM for Type 3: (a) deflection contour, and (b) comparison of experimental and numerical results.

to 1/800 of the supporting span length according to the guidelines of AASHTO and FHWA.

7. Numerical study

The low stiffness of the foam materials used in the cores coupled with relatively short spans often lead to complex behavior at the load and support points. As a result, FEM was used to simulate the behavior of the candidate beam to better understand mechanics of the proposed design. As indicated above, Type 3 beam is recommended for real bridge deck applications based on the results of the experimental work. FEM has shown very good accuracy simulating the complex behavior at the loading points of this beam, as will be explained below.

7.1. Description of the numerical model

The 3-D finite element analysis was conducted using commercial software package ABAQUS/CAE, release 6.11 [46]. The finite element model (FEM) of a representative section of the beam was developed (Fig. 13) and used to predict the flexural behavior of the tested sandwich beams. The Type 3 beam was modeled with the

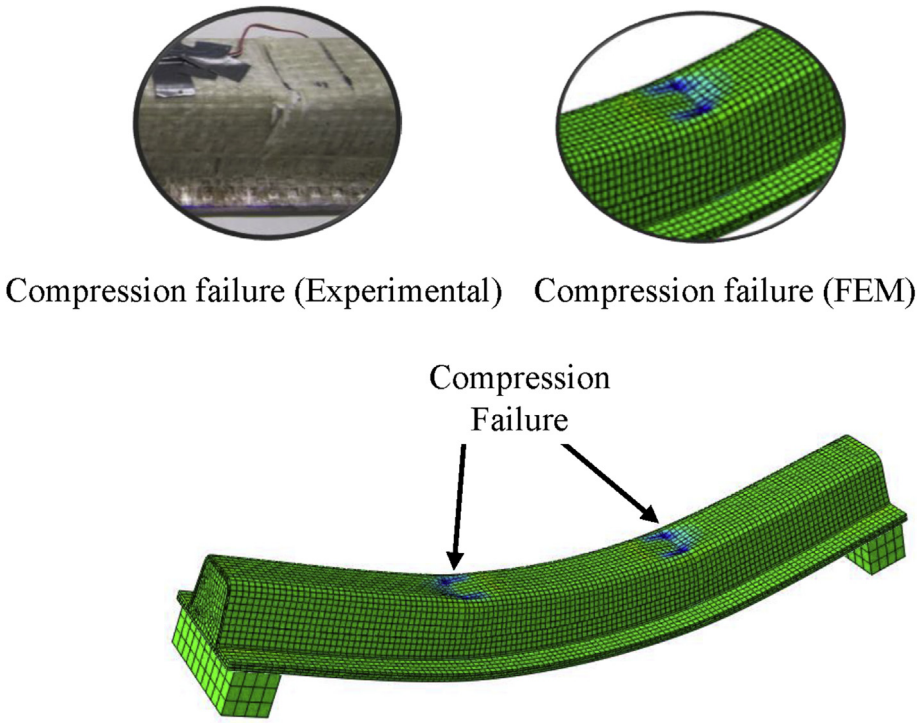

Fig. 15. Failure modes and contours of longitudinal principal stresses. The compressive stresses concentrations at the loading points are observed both in experiments and in FEM.

same geometry (Fig. 1c) as that of the investigated beams. The polyurethane foam, webs, and facings (Fig. 13) were modeled with 3-D continuum solid elements that had eight-node, integration-reduced, linear brick elements (C3D8R, hourglass control). These elements had three translational degrees of freedom (DOFs) at each node. The FRP composites of the facing and web layers have the same volume fraction of the fibers in warp (longitudinal) and fill (transverse) directions. Moreover, the thickness of these layers being small compared to other beam dimensions, consequently the facing and web layers were modeled as isotropic materials to simplify the analysis. The properties were determined from the material characterization tests (Tables 1–3). The polyurethane foam material was modeled using crushable foam model that is available in the ABAQUS library. The crushable foam model has the capability to enhance the ability of a foam material to deform in compression because of the cell wall buckling process [46]. The experimental tests of Type 3 revealed that neither delamination nor relative slip occurred between the facing and the core during testing. Therefore, it is acceptable to assume a full contact (perfect bond) at the interface between the sandwich beam components. The specimen considered in the analysis was loaded and supported by 38.10 mm-wide steel plates, which were free to rotate. The load was applied in displacement control at the metal plates to avoid stress concentration. Contact element was implemented between the loading pads and the GFRP panel. A sensitivity analysis was conducted on the effect of the type of the contact element between the loading pads and the GFRP panel. Two different types of contact elements were investigated: tied contact elements and surface contact element. The first type of contact elements does not allow sliding between the beam surface and loading plate; however, the second contact elements enables such sliding controlled by a coefficient of friction of 0.3. The results of the two models were almost identical; however, the running time of the solution was much lower in the case of tied contact elements. Therefore, tied contact elements were selected for the analysis. The displacement was increased monotonically until the beam failed. The model failed when the FRP materials reached their ultimate tensile or ultimate compressive stress.

7.2. Numerical results

Fig. 14a shows the deflection contours generated using FEM for Type 3 specimen. Fig. 14b illustrates a comparison between the experimentally measured deflection values and the deflection predicted by the FEM at mid-span of the tested beam. Good agreement was observed between the experimental results and the FEM predictions. Overall, the FE model accurately captured the tested sandwich beam's behavior. The sandwich beam reached the peak load of 19.10 kN at the ultimate deflection of 14.22 mm during the experiment. It reached the ultimate load of 20.37 kN at the maximum deflection of 16.25 mm according to the FEM analysis. The average maximum tensile strain at the mid-span's bottom facing recorded during the experiment was equal to 0.0046 mm/mm. For the FEM, this value was 0.0058 mm/mm, a difference of 20%. The FEM tended to slightly overestimate the predicted deflection at mid-span. These differences occurred because of the manufacturing process that produced some variability in the thickness of both GFRP facings and the web layers. Failure in the FEM analysis occurred when the top facing at the applied point loads reached the ultimate stress. This mode of failure matches the experimental behavior (see Fig. 15).

8. Conclusions

The structural behavior of three different core alternatives for GFRP foam-infill sandwich panels was investigated. The results of our experimental and numerical research demonstrated the engineering and economic feasibility of the proposed design.

All sandwich beams tested in bending exhibited a linear-elastic behavior. This initial response was followed with a stiffness

softening prior to failure. The Type 3 construction exhibited better strength as well as flexural and shear stiffness than the other two types investigated in this research. This is due to the remarkable effect of web layers. Also, excellent bond was observed between the polyurethane foam core and the facings in the Type 3 beams.

The Type 3 beams were less vulnerable to localized stress effects under a concentrated load compared to the other two types. On the other hand, Types 1 and 2 were quite susceptible to localized effects under concentrated loads, such as inward local bending and wrinkling of the compression facing under the concentrated loads, which resulted in a lower ultimate strength. Additionally, Types 1 and 2 experienced large deflections associated with significant shear deformation of the core. The Type 3 beam prevented or reduced the facing-core debonding trend that has been observed in conventional sandwich beam construction.

The FEM allowed us to accurately predict the structural behavior of Type 3 beams in bending under monotonic loading, as well as predicting their actual failure modes. Accordingly, this numerical model can be used at the design stage.

Additional work, such as panel-to-panel connections, panel-to-girder joints, roadway crown effect studies, is necessary to facilitate the implementation of the proposed system.

Acknowledgments

The authors acknowledge the financial support provided by the Missouri Department of Transportation (TRyy1203) and the National University Transportation Center (NUTC) (DTRT06-G-0014) at Missouri University of Science and Technology.

References

[1] Kootstookos A, Burchill PJ. The effect of the degree of cure on corrosion resistance of vinyl ester/glass fiber composites. Compos A 2004;35:501–8.
[2] Abdelkarim O, ElGawady MA. Analytical and finite-element modeling of FRP-concrete-steel double-skin tubular columns. J Bridge Engr, ASCE 2015. 40140055-B4014011: B4014005-B4014012.
[3] Dawood H, ElGawady MA. Performance-based seismic design of unbonded precast post-tensioned concrete filled GFRP tube piers. Compos Part B: Eng 2013;44(1):357–67.
[4] ElGawady MA, Dawood H. Analysis of segmental piers consisted of concrete filled FRP tubes. Engr Struct 2012;38:142–52.
[5] Camata G, Shing PB. Evaluation of GFRP honeycomb beams for the O'Fallon park bridge. J Compos Constr ASCE 2005;8(6):545–55.
[6] Davalos JF, Salim HA, Qiao P, Lopez-Anido R, Barbero EJ. Analysis and design of pultruded FRP shapes under bending. Compos Part B Eng 1996;27B:295–305.
[7] Rejab MRM, Cantwell WJ. The mechanical behaviour of corrugated-core sandwich panels. Compos Part B 2013;47:267–77.
[8] Camata G, Shing PB. Static and fatigue load performance of a GFRP honeycomb bridge deck. Comp Part B Eng 2010;41(4):299–307.
[9] Fam A, Sharaf A. Flexural performance of sandwich panels comprising polyurethane core and GFRP skins and ribs of various configurations. Comp Struc 2010;92:2927–35.
[10] Wang L, Liu W, Wan L, Fang H, Hui D. Mechanical performance of foam-filled lattice composite panels in four-point bending: experimental investigation and analytical modeling. Comp Part B Eng 2014;67:270–9.
[11] Correia JR, Garrido M, Gonilha JA, Branco FA. GFRP sandwich panels with PU foam and PP honeycomb cores for civil engineering structural applications: effects of introducing strengthening ribs. Int J Struc Integr 2012;3:127–47.
[12] Noor AK, Burton WS, Bert CW. Computational models for sandwich panels and shells. Appl Mech Rev 1996;49(3):155–99.
[13] Zureick A, Engindeniz M, Arnette J, Schneider C. Acceptance test specifications and guidelines for fiber-reinforced polymeric bridge decks. Washington, DC, Federal Highway Administration: Federal Highway Administration, Georgia Institute of Technology; 2003.
[14] Plunkett JD. Fiber-reinforcement polymer honeycomb short span bridge for rapid installation. IDEA project report. 1997.
[15] Stone D, Nanni A, Myers J. Field and laboratory performance of FRP bridge panels. In: Figueiras J, Juvandes L, Furia R, editors. Compos in Construction, Porto, Portugal; 2001. p. 701–6.
[16] Henderson M. Evaluation of salem avenue bridge deck replacement: issues regarding the composite materials systems used. Final Report. Ohio Department of Transportation; December, 2000.
[17] Reising R, Shahrooz B, Hunt V, Lenett M, Christopher S, Neumann A, et al. Performance of a five-span steel bridge with fiber reinforced polymer composite deck panels. Washington, D.C: Transportation Research Board Annual Meeting; 2001.
[18] Zou B. Design guidelines for FRP honeycomb sandwich bridge decks. Doctoral Dissertation. West Virginia University; 2008 (UMI Number: 3376458).
[19] Davalos JF, Qiao P, Xu XF, Robinson J, Barth KE. Modeling and characterization of fiber-reinforced plastic honeycomb sandwich panels for highway bridge applications. Comp Struct 2001;52:441–52.
[20] Davalos JF, Chen A, Zou B. Performance of a scaled FRP deck-on-steel girder bridge model with partial degree of composite action. Eng Struct 2012;40:51–63.
[21] Potluri P, Kusak E, Reddy TY. Novel stitch-bonded sandwich composite structures. Compos Struct 2003;59(2):251–9.
[22] Hassan T, Reis EM, Rizkalla SH. Innovative 3-D FRP sandwich panels for bridge decks. In: Proceedings of the Fifth Alexandria International Conference on Structural and Geotechnical Engineering. Alexandria, Egypt; 2003.
[23] Reis EM, Rizkalla SH. Material characteristics of 3-D FRP sandwich panels. Constr Build Mater 2008;22(6):1009–18.
[24] Dawood M, Taylor E, Ballew W, Rizkalla S. Static and fatigue bending behavior of pultruded GFRP sandwich panels with through-thickness fiber insertions. Compos Part B 2010;41(5):363–74.
[25] Zureick A. Fiber-reinforced polymeric bridge decks. In: Proceedings of the National Seminar on Advanced Composite Material Bridges, FHWA; 1997.
[26] Bakis CE, Bank LC, Brown VL, Cosenza E, Davalos JF, Lesko JJ. Fiber-reinforced polymer composites for construction state-of-the-art review. ASCE J Compos Constr 2002;2(73):73–87.
[27] Davalos JF, Chen A, Qiaof P. FRP deck and steel girder bridge systems: analysis and design. Boca Raton, FL: CRC Press; 2013.
[28] Keller T, Gurtler H. Composite action and adhesive bond between fiber-reinforced polymer bridge decks and main girders. J Compos Const 2005;9(4):360–8.
[29] Righman J, Barth KE, Davalos JF. Development of an efficient connector system for fiber reinforced polymer bridge decks to steel girders. J Compos Const 2004;8(4):279–88.
[30] Connolly M, King J, Shidaker T, Duncan A. Processing and characterization of pultruded polyurethane composites. Huntsman Enriching lives through innovation. 2006.
[31] Alagusundaramoorthy P, Reddy RV. Testing and evaluation of GFRP composite deck panels. Ocean Eng 2008;35:287–93.
[32] Zenkert D. The hand book of Sandwich Construction. London, UK: Chameleon Press Ltd; 1997. p. 442.
[33] Volz J, Chandrashekhara K, Birman V, Hawkins S, Huo Z, Mohamed M, et al. reportPolyurethane foam infill for fiber-reinforced polymer (FRP) bridge deck panels. Final Report Prepared for Missouri Department of Transportation. Project TRyy1203.
[34] ASTM. A standard test method for flatwise compressive properties of sandwich cores (C365/C365M-11a). Am Soc Test Mater; 2011.
[35] ASTM. A standard test method for tensile properties of polymer matrix composite materials (ASTM D3039/D3039M-08). Am Soc Test Mater; 2008.
[36] ASTM. A standard test method for compressive properties of polymer matrix composite materials with unsupported gage section by shear loading (D3410/D3410M – 08). Am Soc Test Mater; 2008.
[37] ASTM. A standard test method for tensile strength of flat sandwich construction in flatwise plane (C297–08). Am Soc Test Mater; 2008.
[38] ASTM. A standard test method for flexural properties of sandwich constructions (C393/C393M-11e1). Am Soc Test Mater; 2011.
[39] Wyoming Test Fixtures INC. Long beam flexure test Fixture. <http://www.wyomingtestfixtures.com/Products/d2.html> [22.07.2014].
[40] Carlsson LA, Kardomateas GA. Structural and failure mechanics of Sandwich composites. Springer; 2011.
[41] Newmark NM, Siess CP, Viest IM. Tests and analysis of composite beams with incomplete interaction. Proc Soc Exp Stress Anal 1951;9(1):75–92.
[42] Faella C, Martinelli E, Nigro E. Steel–concrete composite beams in partial interaction: closed-form "exact" expression of the stiffness matrix and the vector of equivalent nodal forces. Eng Struct 2010;32:2744–54.
[43] Gibson LJ, Ashby MF. Cellular solids: structure and properties. Oxford: Pergamon; 1988.
[44] Tuwair H, Volz J, ElGawady M, Mohamed M, Chandrashekhara K, Birman V. Testing and evaluation of GFRP sandwich bridge deck panels filled with polyurethane foam. In: The American Society for Composites 29th Technical Conference, 16th US-Japan Conference on Composite Materials, and ASTM D-30 Meeting, San Diego, CA, Sept; 2014.
[45] AASHTO. LRFD bridge design specifications. 6th ed. Washington, D.C: Am Soc of State Highway Tran; 2013. Interim Revisions.
[46] ABAQUS software and documentation. V.6.11–1. SIMULIA: ©Dassault Systèmes; 2013.